A NEW CLIMATOLOGY OF THE AEROSOLS BASED ON THEIR INHERENT OPTICAL PROPERTIES FOR THE MERIS ATMOSPHERIC CORRECTIONS OVER OCEAN

Francis ZAGOLSKI [(1)], Richard SANTER [(2)], and Ouahid AZNAY[(2)]

(1) ADRINORD, Association pour le Développement de la Recherche et de l'Innovation dans le NORD, 2 rue des Canonniers, Lille, F59000 – FRANCE.
E-mail: Francis_Zagolski@yahoo.ca

(2) ULCO, Université du Littoral Côte d'Opale – UPRES-A8013 ELICO/CNRS, 32 Avenue Foch, Wimereux, F62930 – FRANCE.
E-mails: Richard.Santer@mren2.univ-littoral.fr, Ouahid.Aznay@mren2.univ-littoral.fr

ABSTRACT

In the classical scheme of atmospheric corrections over oceans, the derivation of aerosol path radiances in the visible region is achieved using aerosol models deduced from the spectral dependency of atmospheric signals in the near-infrared domain. Standard models are generally included in the aerosol climatology, but the latter is not sufficient to describe variety of aerosols encountered over coastal areas. One way to extend this climatology consists in the generation of additional models.

Coastal and inland CIMEL stations from AERONET (AErosol RObotic NETwork) offer an extensive data set of aerosol characteristics in marine environment through solar extinction and sky radiance measurements. Data collected by 25 stations during several years have been processed with an iterative method of aerosol phase functions retrieval developed at ULCO, to build-up a very large database (~7000 sequences). Statistical methods applied on this data set allowed to discard the wrong sequences and to suggest a classification in aerosol models through their inherent optical properties.

1. INTRODUCTION

The approach developed to build-up a new aerosol climatology focuses on the use of MERIS (MEdium Resolution Imaging Spectrometer), but it can be easily generalized to any other sensors working in the solar spectrum for atmospheric corrections both over land and water surfaces. The objective of this work is to bring some recommendations for generating a new set of look-up tables (LUT's) in the current MERIS algorithm both for the aerosol remote sensing and the atmospheric corrections over oceans.

1.1 Atmospheric corrections over ocean

MERIS, on the ENVISAT plateform (launched on March 1st, 2002), is a medium-spectral resolution imaging spectrometer operating in the solar reflective spectral range $[400\,nm - 900\,nm]$. Fifteen spectral bands can be selected by ground command, with a programmable width and spectral location. The scene is simultaneously registrated across the entire spectral range through a dispersing system onto a CCD array.

The top of atmosphere (TOA) radiance (L) measured by MERIS and delivered as the level-1 product needs to be transformed before to be used in the level-2 processing. Radiances are firstly normalized by considering an extraterrestrial solar irradiance equal to π:

$$L_n = L \cdot \frac{\pi . d^2}{E_s}, \qquad (1)$$

in which E_s is the solar irradiance corrected for the *Sun-Earth* distance d (in *A.U.*), for the central wavelength of each spectral band. This conversion is critical for MERIS because of the so-called smile effect which induces a variation of E_s within the field of view for any spectral bands. E_s being known for each pixel, a spectral adjustment is achieved to propose a normalized radiance for the central wavelength of each MERIS band.

A second step consists in the gaseous absorption removal from the normalized TOA radiances. These absorbing effects mainly result from the stratospheric ozone and the water vapor. The ozone layer being located above the aerosols, this gaseous correction is completed by decoupling the absorption and scattering processes. The ozone transmissivity is calculated as a decreasing exponential law which depends on the ozone optical thickness precomputed in each spectral band for a standard ozone content ($0.32\,cm\text{-}atm$) and weighted by the actual ozone amount provided by the European Centre for Medium range Weather Forecast (ECMWF). The water vapour (mostly located in the lower troposphere) correction is achieved according to [1].

Finally, because the MERIS level-1 product is the remote sensing reflectance for ocean, we convert the normalized TOA radiance (L_n) into reflectance (ρ^*):

$$\rho^* = \frac{L_n}{\mu_s \cdot T_g}, \qquad (2)$$

where T_g is the total gaseous transmittance and μ_s the cosine of the solar zenith angle.

In ocean colour remote sensing, the TOA reflectance corrected for gaseous absorption can be linearized as:

$$\rho^* = \rho_{atm} + T \cdot \frac{\rho_w}{1 - \rho_w \cdot S} + \rho_G \cdot e^{-M \cdot \tau}, \qquad (3)$$

where ρ_{atm} stands for the intrinsic atmospheric contribution (multiple scattering contributions from the molecules, the aerosols and the *Rayleigh-aerosol* coupling, as well as from the coupling between atmospheric scattering and *Fresnel* surface reflection), T the total atmospheric transmittance (*Rayleigh* + aerosol), S the spherical albedo relating to the molecules and the aerosols, τ the total optical thickness (*Rayleigh* + aerosol), M the airmass, and ρ_w and ρ_G, respectively the water-leaving reflectance and the aerosol/molecules-ground system reflectance (*i.e.*, the glitter at the *air-sea* interface). The *Fresnel* reflection is accounted for in the computation of the coupling terms between *Fresnel* reflection and atmospheric scattering, but the *Fresnel* reflection for the direct to direct path is removed.

Over case-1 waters as defined in the MERIS ocean product, ρ_w is considered as null both at $778.75\,nm$ and $865\,nm$. Outside of the sun glint area, the TOA signal corresponds to the intrinsic atmospheric scattering only. Consequently, from the two atmospheric path radiances (acquired at $778.75\,nm$ and $865\,nm$) we can retrieve the aerosol type and the aerosol optical thickness (AOT) at $865\,nm$ (see [2] for more details).

1.2 The MERIS standard aerosol models (SAM's)

The aerosol types are provided by the climatology. Models from the SeaWiFS (Sea-viewing Wide Field-of-view Sensor) climatology were used in the first MERIS processing [2]. The latters consist in 12 models of *Shettle & Fenn*: four types of aerosols (maritime, coastal, tropospheric and urban) with three relative humidities (70%, 90% and 98%). In the following sections, we will refer to a given aerosol model by using the first letter of the model type and the relative humidity (expressed in percent) as notation. For example, M70 stands for the maritime model with a relative humidity of 70%. Among all these models, only the urban type presents some absorption.

An updated set was suggested for the second MERIS reprocessing with the same maritime and coastal models but for four relative humidities (50%, 70%, 90% and 99%). The rural aerosols are slightly less absorbing than the previous urban models. Another major point is the introduction of the so-called blue (BL) aerosol models. The latters account for the strong spectral dependency of the AOT as reported by several authors. The land aerosol models from [1] were employed. They are described by a *Junge* size distribution $n(r)$:

$$n(r) \approx r^{\alpha - 3}, \qquad (4)$$

with r the particle radius and α the *Angström* exponent describing the wavelength dependency of AOT ($\tau_a(\lambda)$):

$$\alpha(\lambda, \lambda') = \frac{Log(\tau_a(\lambda)/\tau_a(\lambda'))}{Log(\lambda/\lambda')}. \qquad (5)$$

Four values of α (-1.5, -2, -2.5, -3) were implemented in the MERIS level-2 processing.

For each model, the aerosol optical properties were computed with the *Mie*'s theory and a refractive index (m) of 1.44 as default value, in 13 MERIS bands (two strong O2 and H2O absorption bands were discarded):

- the extinction coefficient (σ_a) and the scattering coefficient or the single scattering albedo (ω_a),
- the phase function $P_a(\Theta)$ versus scattering angle (Θ).

Actually, to generate the LUT's required for the atmospheric corrections over ocean, we calculated for each aerosol type:

- the ratio of extinction coefficients $\sigma_a(\lambda)/\sigma_a(865)$ between λ and a reference wavelength at $865\,nm$,
- the single scattering albedo times the phase function, $\omega_a(\lambda).P_a(\Theta,\lambda)$.

Tab. 1 summarized the α values for the SAM's used in the second MERIS reprocessing.

Table 1: *Spectral dependency of the MERIS aerosol models in the near-infrared region.*

Model	*M50*	*M70*	*M90*	*M99*	*C50*	*C70*	*C90*	*C99*
-α(665,865)	0.51	0.41	0.20	0.08	0.78	0.66	0.40	0.22

Model	*R50*	*R70*	*R90*	*R99*	*BL1*	*BL2*	*BL3*
-α(665,865)	1.67	1.66	1.51	1.30	1.50	2.00	2.50

1.3 Retrieval of inherent optical properties (IOP's)

Based on the use of the CIMEL instrument, we firstly derived the AOT's and the spectral dependency of the extinction coefficient. Then, we followed the inversed method of the sky radiance from [3] to derive the aerosol single scattering albedo times the phase function ($\omega_a.P_a(\Theta)$). This method has been applied for several days on the in-flight calibration of MERIS [4], in the red and near-infrared regions. The increasing role of the *Rayleigh* scattering emphasized the influence of the aerosol vertical distribution and this parameter has been introduced in the inversion scheme.

What we use in this study is an updated version of this algorithm [5], which first brings some improvements in the radiative transfer computations with the successive orders (SO) of the scattering code [6]. Second, the vertical distribution of the aerosols is introduced using an exponential law with a vertical scale height (H_a).

The inputs for the nominal inversion are the followings:

- an aerosol scale height (H_a) of $3\,km$,
- a dark water surface and a *Fresnel* reflection driven by a wave slope distribution induced by a wind-speed of $7.2\,m/s$,
- an iterative process initiated with a *Junge* phase function corresponding to α=-1, and a refractive index m=1.44 without any absorption.

2. AEROSOL IOP's DERIVED FROM CIMEL MEASUREMENTS

The CIMEL E-318 sun-photometer is fitted with four filters at 1020*nm*, 870*nm*, 675*nm* and 440*nm* for measuring atmospheric aerosol optical properties. This instrument presents three scanning protocols: (*a*) *sun*, (*b*) *almucantar*, and (*c*) *principal plane* (*ppl*) (see [7] for more details). Only the *sun* and *ppl* protocols of sky radiance measurements have been used here to retrieve the aerosol optical properties. The AOT's are derived from the extinction measurements.

2.1 CIMEL database

More than 90000 CIMEL data sequences were downloaded from the AERONET (AErosol RObotic NETwork) web-site. These measurements (extinctions and *ppl* sky radiances) were collected by 25 stations selected over the world from years 1998 to 2003. This data set yields to a number of AOT's larger than 500000 for the same period.

Before to be processed in the phase function retrieval algorithm, the data set has been filtered to keep only the sequences for which the solar zenith angle (θ_s) is larger than 65*deg*. and for which the AOT's and sky radiances are correctly measured and recorded at 440*nm*, 675*nm* and 870*nm*. An output sequence from the iterative process consists in *Angström* exponents, α(440,870) and α(675,870), ω_a and $P_a(\Theta)$ at 675*nm* and 870*nm*.

2.2 Outputs from the data processing

Following aerosol optical properties are derived from the CIMEL measurements:

- the AOT's (τ_a) at 440*nm*, 675*nm* and 870*nm*, from which is deduced $\sigma_a(\lambda)/\sigma_a(865)$ using the *Angström* exponent (α) determined either between 440*nm* and 675*nm*, or 675*nm* and 870*nm*,
- the aerosol single scattering albedo times the phase function ($\omega_a.P_a(\Theta)$) at 675*nm* and 870*nm* for 80 *Gaussian* scattering angles.

A data filtering has been applied on the initial set of 7109 sequences. The sky radiance at the scattering angle of 6*deg.* is measured twice with two different gains. Actually, the *sun* collimator is selected for Θ lower than 6*deg.* whereas the *sky* collimator is used for Θ larger than 6*deg.* If the two radiances differ by more than 10%, then the sequence is rejected. If not, only the *sky* collimator measurement is considered. Thus, the validation of this angular smoothness on $\omega_a.P_a(\Theta)$ yielded to the selection of 3157 sequences. This data set was still reduced to 2171 sequences after applying two other criteria on the *Angström* exponents and on the single scattering albedos which allowed to account for the errors resulting from the calibration uncertainties:

$$-2.5 \le \alpha \le 0.5 \text{ and } 0.6 \le \omega_a \le 1.05 \qquad (6)$$

3. FIRST ANALYSES OF THE DATABASE

The spectral dependency of the AOT between 675*nm* and 870*nm* allows us to select an aerosol model. The AOT at 870*nm* is then extrapolated in the blue region. Fig. 1 relates the spectral dependency between the two *Angström* exponents. As expected, for small values the plot is scattered (near zero division).

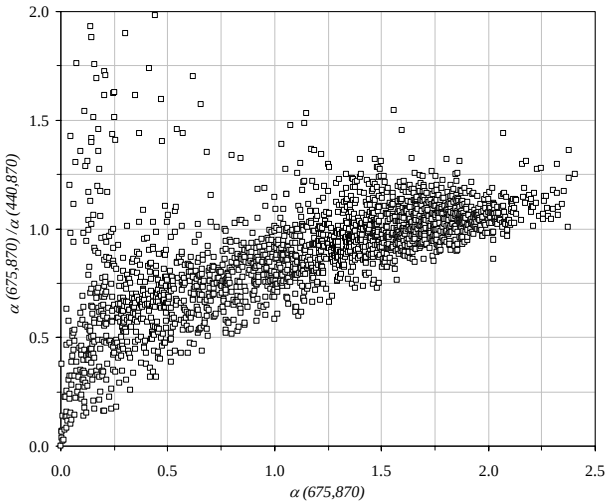

Figure 1: *Spectral dependency between α(440,870) and α(675,870).*

Same analysis was conducted on the single scattering albedos derived from all the sky radiances measured at 870*nm*. Results stress that the distribution of ω_a(870) versus α(440,870) is quite scattered because of the poor accuracy on this determination. Both for the two wavelengths (675*nm* and 870*nm*) the average value of α is around to -1.1. Mean values of ω_a are 0.899 and 0.883, respectively at 675*nm* and 870*nm*.

The aerosol transmittivity $T_a(\mu,\lambda)$ is expressed as:

$$T_a(\mu,\lambda) = \exp\left[-\left(1-\omega_a(\lambda)\cdot F_a(\mu,\lambda)\right)\cdot\frac{\tau_a(\lambda)}{\mu}\right], \qquad (7)$$

where $F_a(\mu,\lambda)$ represents the aerosol forward scattering proportion. The latter is computed using the retrieved aerosol phase function $P_a(\Theta,\lambda)$ as follows:

$$F_a(\mu,\lambda) = \frac{1}{4\pi}\int_0^1\int_0^{2\pi} P_a(\Theta,\lambda)\cdot d\mu'\cdot d\phi, \qquad (8)$$

in which, the incident direction is defined by (μ,ϕ) and the diffused direction by (μ',ϕ'), $d\phi$ corresponding to the difference in azimuth between ϕ and ϕ'. Because Eq.8 is usually employed in most of atmospheric correction algorithms, the derivation of F_a from the sky radiance measurements is of concern.

Angular and spectral dependencies of the aerosol forward scattering proportion $F_a(\mu,\lambda)$ are presented in [5]. In summary, F_a slightly decreases as function of θ_s and no trend appears between F_a and α.

4. AEROSOL CLIMATOLOGY BASED ON IOP's

4.1 Classification of phase functions

The influence of the AOT on the aerosol phase function retrieval is illustrated in Fig. 2. Results are depicted for α=-1.5±0.1 both at 675*nm* and 870*nm* and for a scattering angle of 90*deg.*. We can note that no trend appears on the phase function versus the AOT when the plots are scattered. This was also observed for other Θ values. Consequently, the robustness of the inversion scheme is checked within the range of the encountered aerosol loadings. This analysis has been deeply investigated for the full range of α and the results confirmed what we obtained for α=-1.5.

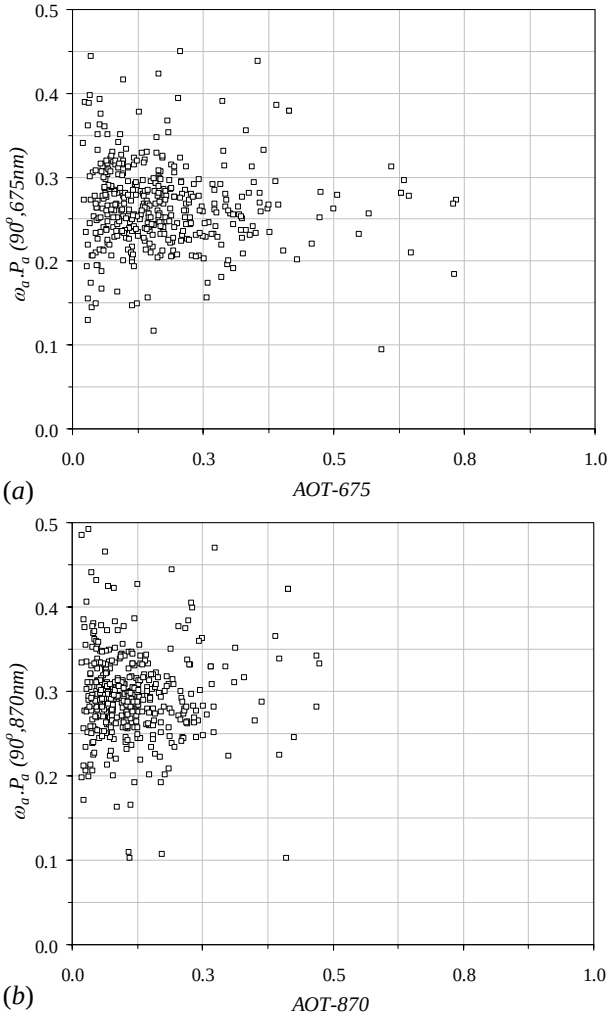

Figure 2: *Influence of the AOT on the retrieved aerosol phase function* $\omega_a.P_a(\Theta)$. *Results are reported for the class corresponding to* $<\alpha>$ *=-1.5±0.1, at 675nm (a) and 870nm (b) for* $\Theta=90^o$.

Fig. 3 displays variation of $\omega_a.P_a(90^o)$ with α. Although the plots are scattered, this result indicates an expected trend. In fact, the phase function normally increases when the particle size become smaller.

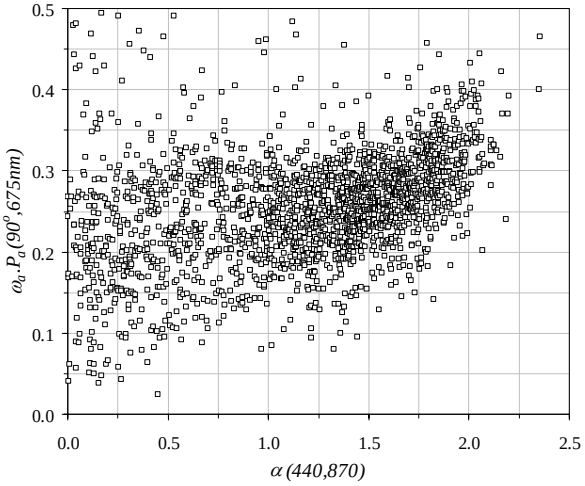

Figure 3: *Aerosol phase function* $\omega_a.P_a(90^o)$ *at 675nm expressed as function of* α*(440,870).*

Selection of one aerosol type is based on α. As the aerosol IOP's appear to be continuous versus α, then we characterized the latters by α classes: α is selected within [-2.5;0] by step of 0.1 (except for the last value which is fixed to 0.05) with a $\Delta\alpha$ of 0.2 (*resp.*, 0.1 for the last value) centred on the nominal value. For these 25 classes, in the Θ range of [0-150]*deg.*, the retrieved $\omega_a.P_a(\Theta)$ are averaged by class of α. Tab. 2 gives the number N_0 of $\omega_a.P_a(\Theta)$ at 675*nm* per class of α. A filtering technique has been applied on these phase functions for each class. For that, we computed the root mean square error (*rms*, denoted as σ_0) on $\omega_a.P_a(\Theta)$ for each Θ. A filtering is then achieved for each Θ at one σ_0, which reduces the number of phase functions to N_1 for each class of α. This process is achieved twice. Tab. 2 displays the mean value of *rms* for Θ ranged in [100-150]*deg.* After the second round, the *rms* value (σ_1) indicates the mean absolute accuracy on the retrieved aerosol phase function.

Table 2: *General features of mean* $\omega_a.P_a(\Theta)$ *at 675nm:* $<\alpha>$ *is the mean value of* α *(*$\Delta\alpha$*= 0.2),* N_0 *(resp.,* N_1*) the number of phase functions per class of* $<\alpha>$ *(resp., after applying a filter at* 2σ*).* $<\sigma_0>$ *is the mean value of rms computed on the phase function for each* Θ *within [100-150] deg., and* $<\sigma_1>$ *the mean of rms on the filtered set of phase functions.*

$<\alpha>$	0.05	0.1	0.2	0.3	0.4	0.5	0.6	0.7	0.8	0.9	1.0	1.1	1.2
N_0	70	182	215	188	184	167	146	153	139	154	190	209	217
N_1	65	169	200	178	173	157	136	140	130	144	178	195	204
$<\sigma_0>$	0.18	0.17	0.17	0.15	0.10	0.10	0.12	0.13	0.11	0.08	0.06	0.07	0.09
$<\sigma_1>$	0.10	0.08	0.08	0.07	0.06	0.06	0.06	0.06	0.05	0.05	0.04	0.04	0.05

$<\alpha>$	1.3	1.4	1.5	1.6	1.7	1.8	1.9	2.0	2.1	2.2	2.3	2.4
N_0	231	247	253	262	263	254	200	132	84	41	30	12
N_1	218	233	238	248	249	239	188	126	79	37	28	11
$<\sigma_0>$	0.08	0.09	0.09	0.08	0.07	0.06	0.06	0.06	0.05	0.04	0.06	0.08
$<\sigma_1>$	0.04	0.05	0.05	0.04	0.04	0.04	0.04	0.04	0.04	0.03	0.04	0.03

4.2 Accuracy on the IOP's

The initial work from [3] reported some outputs for the sensitivity study based on theoritical predictions. The phase function was retrieved at 870 *nm* only, for an homogeneous atmosphere. The saillant point was that the relative error on the radiometric calibration results in the same amount of the relative error on the retrieved phase function. What we conduct here is a sensitivity study on the inversion of the full CIMEL database to the following individual parameters:

- CIMEL sky radiance measurements are multiplied by 1.03 to account for a systematic error of 3 percent in the downwelling radiance calibration,
- an aerosol scale height (H_a) of 1 *km*,
- a wave slope distribution induced by a wind of 3 *m/s*,
- an initial phase function computed with the *Junge* size distribution corresponding to α=-1, and a refractive index m=1.33 without any absorption.

Fig. 4 displays the impact of the error introduced in the data calibration on the retrieval of the aerosol phase function ($\omega_a.P_a(\Theta)$) at 675 *nm* for a scattering angle of 120 *deg*. Each individual $\omega_a.P_a(\Theta=120,3\%)$ derived from sky radiance including the systematic error of 3% is plotted as function of its associated nominal one (*i.e.*, without introducing an error). As expected, the results stress that the plots are few scattered and remain very close to the bissector with a slight overestimate in the case of the introduction of the systematic error. Same results were observed at 870 *nm*. Tab. 3 reports the influence of this error in the data calibration on $F_a(\mu,\lambda)$ at two solar zenith angles (30 *deg* and 60 *deg*) and on $\omega_a.P_a(\Theta)$ for a scattering angle of 90 *deg.*, 110 *deg.*, 130 *deg.*, and 150 *deg.* We first give the mean of the ratio R defined as:

$$R(\Theta,\lambda,calib.) = P_a(\Theta,\lambda,3\%)/P_a(\Theta,\lambda,0\%), \quad (9)$$

and its associated *rms* value.

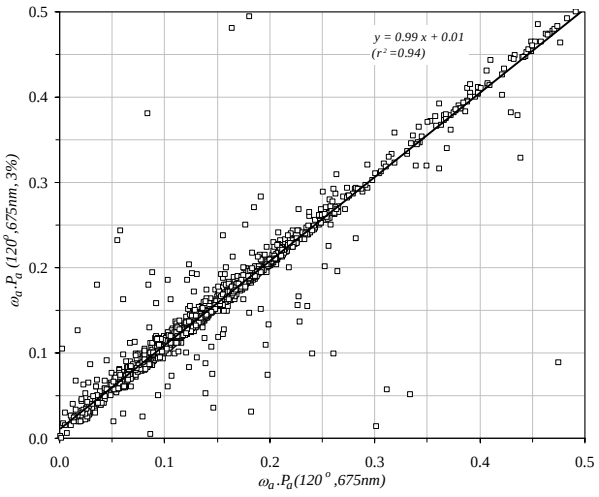

Figure 4: *Impact induced by an error of 3% introduced in the CIMEL data on the retrieval of $\omega_a.P_a(120^o)$ at 675 nm.*

The same approach has been applied for the aerosol scale height, the wind-speed above sea level, and the refractive index of the aerosol model. All the results for the 675 *nm* wavelength are reported in Tab. 3.

Table 3: *Outputs from the sensitivity study at 675 nm on $\omega_a.P_a(\Theta)$ for several scattering angles (Θ) and on $F_a(\theta_s,\lambda)$ for two solar zenith angles (θ_s): δ is the relative error between $\omega_a.P_a(\Theta)$ retrieved from sky radiance including an error induced by either the data calibration (calib.), or the aerosol refractive index (m), or the aerosol scale height (H_a), or the wind-speed (w_s), and its nominal value. <R> represents the mean value of the ratio between retrieved and nominal phase functions, and σ its associated rms error.*

	$\omega_a.P_a(90^o)$	$\omega_a.P_a(110^o)$	$\omega_a.P_a(130^o)$	$\omega_a.P_a(150^o)$	$F_a(30^o)$	$F_a(60^o)$
$\delta_{calib.}$(%)	9.0	16.5	21.5	10.8	10.0	18.4
$<R_{calib.}>$	1.035	1.063	1.048	1.030	1.032	1.037
$\sigma_{calib.}$	0.024	0.038	0.037	0.030	0.018	0.023
δ_m(%)	3.5	9.1	11.4	8.1	3.5	4.8
$<R_m>$	0.998	0.983	0.983	1.005	1.001	1.003
σ_m	0.003	0.013	0.008	0.012	0.005	0.008
δ_{H_a}(%)	2.0	5.9	7.6	5.9	0.7	1.1
$<R_{H_a}>$	1.011	1.015	1.063	0.968	1.000	1.003
σ_{H_a}	0.011	0.015	0.016	0.015	0.006	0.008
δ_{w_s}(%)	4.4	7.0	12.8	8.0	1.4	1.5
$<R_{w_s}>$	0.981	0.974	0.965	0.966	0.992	0.991
σ_{w_s}	0.012	0.016	0.018	0.013	0.005	0.006

Conclusions of this sensitivity study at 675 *nm* and 870 *nm* are mostly based on the analysis of R:

- The calibration of the sun-photometer is a key issue. Any multiplicative bias is reported in proportion on the aerosol phase function if we are close to the single scattering regime and if the *Rayleigh* scattering can be neglected which is more or less the case at 870 *nm*. At 675 *nm*, the situation is more complex to analyze but the multiplicative bias is still of the order of the calibration bias.
- It was expected to observe no impact from the initial guess of the aerosol phase function in the iterative process which quickly converges. This is especially the case in the forward scattering on the F_a factor because first, the scattering regime is close to the primary one and second, the diffraction peak does not depend upon the particle refractive index. In the backscattering region, the influence of the refractive index observed on the retrieval results from the non-knowledge of the phase function for scattering angles larger than 150 *deg*. The backscattering domain is sensitive to the refractive index and the result clearly illustrates the uncertainty due to the non-access to the forward scattering. Nevertheless, this effect remains quite small.

- The effect of the vertical distribution is negligible in the forward scattering region where the aerosol scattering dominates. This is still small in the backscattering region even at 675*nm* where the influence of the *Rayleigh* scattering increases. On the other hand, this impact can be cancelled if the same aerosol vertical distribution is assumed both for this phase function retrieval and in the atmospheric correction algorithm.

- The larger the wind-speed is and the larger is the amount of reflected light due to the fact that the direct sun glint invokes more grazing incident angles with high *Fresnel* reflection coefficient. The F_a factor is not much sensitive to the wind-speed because of the strong forward scattering. On the aerosol phase function, the errors of a few percents invite to account for the wind-speed in our analysis.

4.3 Spectral dependency of the IOP's

To conduct this study, it is mandatory to well know the aerosol phase functions in the different spectral bands. Over ocean, the aerosol remote sensing algorithm is based on the use of the aerosol path radiances for the doublet (670*nm* and 870*nm*) or (770*nm* and 865*nm*). CIMEL measurements are available at 675*nm* and 870*nm*. Assuming that the spectral dependency on the measurements remains quite smooth in this near-infrared region, the radiance at 770*nm* can then be easily obtained by applying a spectral interpolation. Fig. 5 depicts the ratio of $\omega_a.P_a(\Theta)$ computed between 675*nm* and 870*nm*. Firstly, we can note that in the case where all the individual measurements are considered (Fig. 5*a*), these ratios are well peaked around the one value, but nevertheless they remain quite scattered. Secondly, by averaging $\omega_a.P_a(\Theta)$ by class of α (Fig. 5*b*) this dispersion is strongly reduced. Then, we accounted for the particle size, through α, by suggesting a spectral dependency on $\omega_a.P_a(\Theta)$ for different scattering angles. This is illustrated in Fig. 5*c* which clearly stresses a trend on the ratio of $\omega_a.P_a(\Theta)$ with α.

When dealing with the atmospheric corrections for ocean colour, we need to know the phase function in the blue region. As reported by [5], the retrieval of the aerosol phase function ($\omega_a.P_a(\Theta)$) is more challenging and some limitations clearly occur for large AOT's and low solar elevations. Despites this, we launched the inversion scheme in the blue region on the full data set to finally retrieve $\omega_a.P_a(\Theta)$ at 440*nm*. The same classification on α has been achieved and we analyzed the spectral dependency on $\omega_a.P_a(\Theta)$ between 440*nm* and 675*nm*. The significance of these results was more questionable because of the high dispersion (some points are out of scale). Consequently we suggest to extrapolate the results from 675*nm* and 870*nm* for estimating $\omega_a.P_a(\Theta)$ at 440*nm*.

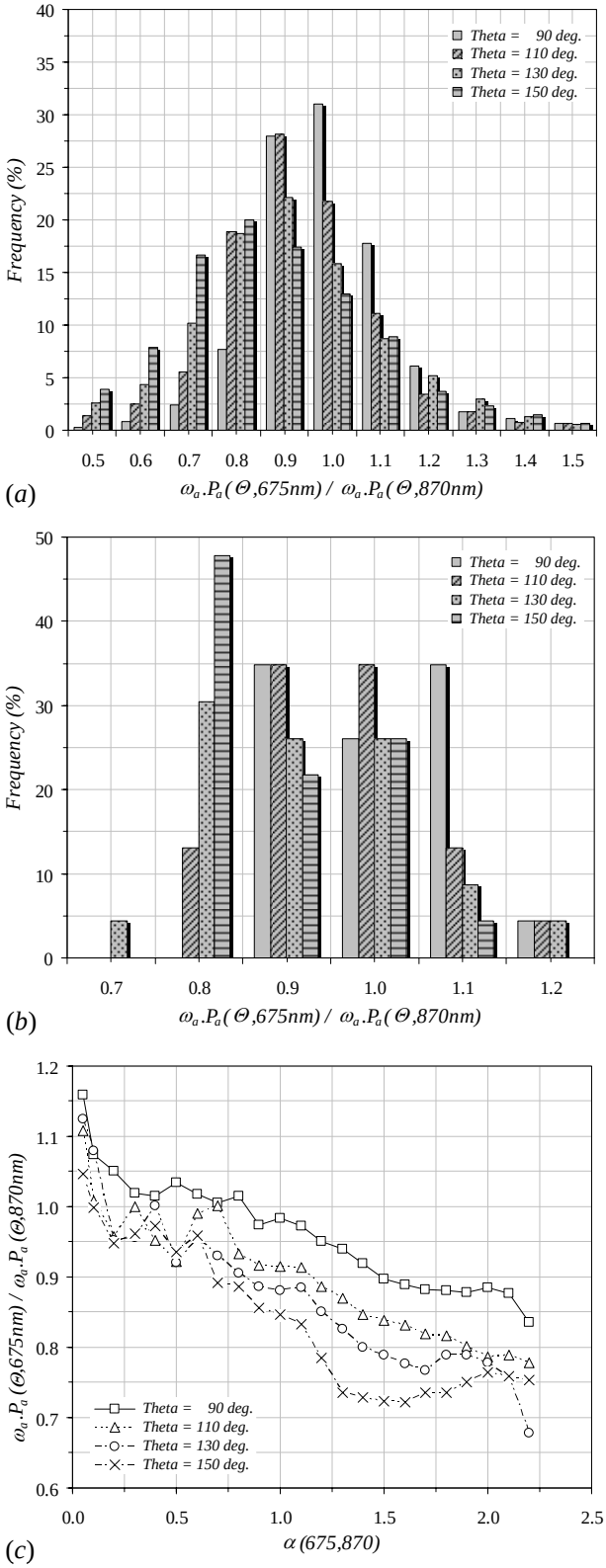

Figure 5: *Histogram of ratio of* $\omega_a.P_a(\Theta)$ *computed between 675 nm and 870 nm for 4 scattering angles* (Θ=90°, 110°, 130°, *and* 150°). *Results depicted in figure (a) derive from all individual CIMEL measurements, whereas figure (b) is for the averaging of* $\omega_a.P_a(\Theta)$ *by classes of* α. *Figure (c) displays the spectral dependency of this ratio.*

4.4 Comparison between simulated and measured phase functions

Two sets of aerosol phase functions were available: the first one was computed for the MERIS SAM's, and the second one results from the CIMEL sky radiance analysis. Comparison between these two sets of phase functions at 870 *nm* for some samples of aerosol models (maritime, rural, coastal and land) stressed that the predicted aerosol phase function may underestimate by a factor of two within the MERIS range of scattering angle (*i.e.*, [100-150] *deg.*). Only the *Junge* size distribution which was employed for simulating the so-called blue aerosols, well compared. Works from [8] proposed to use *Junge* size distributions for the atmospheric corrections over ocean, which appears here to be a reasonable alternative to the MERIS SAM's.

4.5 Consequences on the MERIS aerosol product

In the framework of MERIS activities, some validations of the aerosol product over ocean based on the use of CIMEL data are reported in [9]. Results are summarized in Tab. 4. From ground-based measurements, we directly compare the AOT's at 870 *nm* with MERIS AOT's at 865 *nm*. For each of the 14 validation days, α(675,870) is computed with the CIMEL sequence nearest to the time of MERIS overpass. The latter is then compared to α(665,865) derived from MERIS.

Table 4: *AOT at 865/870 nm and α for CIMEL acquisitions and the two MERIS processings.*

		1st Process		*CIMEL*		*2nd Process*	
Site	*Date*	*AOT*	α	*AOT*	α	*AOT*	α
Venise	10/08	0.22	-1.111	0.29	-0.870	0.20	-0.993
Venise	13/08	0.18	-1.489	0.22	-1.780	0.08	-2.439
Lampedusa	20/08	0.24	-0.567	0.21	-0.990	0.20	-0.587
Gotland	07/09	0.07	-0.673	0.04	-0.730	0.09	-0.423
Gotland	08/09	0.06	-1.052	0.06	-0.710	0.07	-0.751
Helgoland	16/09	0.22	-0.442	0.15	-1.150	0.16	-1.252
Lampedusa	21/09	0.13	-0.665	0.06	-1.860	-	-
Venise	16/10	0.10	-0.950	0.05	-0.670	0.07	-0.588
Venise	25/10	0.12	-1.585	0.05	-1.200	0.08	-0.811
Calcofi	28/10	0.14	-1.497	0.06	-1.600	0.09	-1.653
Venise	04/11	0.11	-0.673	0.05	-1.370	0.07	-0.990
Calcofi	10/11	0.14	-0.205	0.06	-0.360	0.07	-0.529
Venise	10/11	0.13	-0.629	0.04	-0.460	0.08	-0.778
Venise	13/11	0.15	-0.532	0.11	-1.580	0.16	-1.284

The good agreements observed on α for the 2nd MERIS reprocessing can be explained by the fact that we do not require any assumption on the SAM's as far as the spectral dependency of $\omega_a.P_a(\Theta)$ can be neglected. This reflects the ability to properly extract the aerosol path radiance over dark oceans. Except for Venice site (August 13th, 2003), the MERIS aerosols appear whiter than they should be. Poor results obtained with the 1st processing are surely due to the fact that the initial family of SAM's is not representative of the full range of observed α. The MERIS AOT's remain quite poor both for the two processings. MERIS systematically overestimates the AOT by a factor around to 2.

As a first attempt to introduce our new aerosol climatology in the MERIS atmospheric correction algorithm, we firstly assumed that the latter correctly extracts from the TOA signal the normalized aerosol path radiance at 865 *nm* in the primary scattering approximation.

In order to use our IOP's, we process with these steps:

- The *Angström* exponent derived from the MERIS level-2 allows to select two SAM's using Tab. 1.
- The optical properties of the aerosol model $(\omega_a.P_a(\Theta))_{SAM}$ employed in the MERIS level-2 are obtained by interpolation on α.
- The *Angström* exponent derived from the MERIS level-2 allows to select our IOP's data $(\omega_a.P_a(\Theta))_{IOP}$.
- Using the primary scattering approximation, we get a new AOT value which will be consistent with the new aerosol IOP's:

$$L_a^{(1)}(\mu,\lambda) = \frac{\left(\tau_a(\lambda)\cdot\omega_a(\lambda)\cdot P_a(\Theta,\lambda)\right)_{SAM}}{\left(\omega_a(\lambda)\cdot P_a(\Theta,\lambda)\right)_{IOP}}, \quad (10)$$

Fig. 6 compares the AOT at 665 *nm* derived from MERIS in the two ways (*i.e.*, with the SAM's and with the IOP's) and from the CIMEL measurements at 675 *nm* over the *Lampedusa* site for several validation days. A linear regression applied on each of the two data sets indicates that the MERIS AOT estimate is slightly improved with the IOP's. However, this was not observed in the near-infrared region over the same site, for which the MERIS standard aerosol product is much more overestimated than the one at 665 *nm*. Although these results are not conclusive, this methodology suggested for validating the impact of the new aerosol IOP's on the aerosol product easily applies.

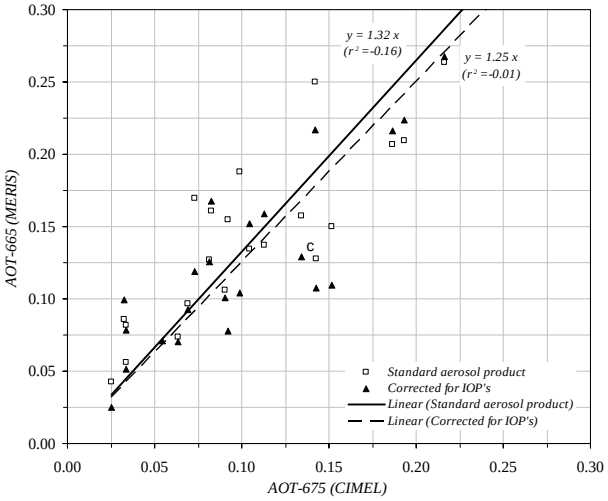

Figure 6: *MERIS AOT at 665 nm (from standard aerosol product and from correction for IOP's) versus CIMEL AOT at 675 nm, over Lampedusa.*

5. CONCLUSION

Aerosol remote sensing and atmospheric schemes require to rely on SAM's which enable to know the standard aerosol IOP's. The AERONET offers an unique opportunity to describe these IOP's. The spectral dependencies of the AOT's are directly available from the extinction measurements. An algorithm to derive the aerosol phase function from the sky radiances was available to us. Our major task was to select and process a significant amount of CIMEL sequences. For this database, we proposed a set of IOP's both for the aerosol remote sensing and the atmospheric correction.

Limitations to this work are well identified. The CIMEL data were processed using a radiative transfer code assuming a plane parallel atmosphere even if low solar elevations and grazing view angles are involved, and an homogeneous system while some CIMEL stations are located on the coastline which may imply the so-called adjacency effects in the measurements. Moreover, these computations were completed with some standard inputs (a barometric pressure of $1013\,hPa$, a standard climatologic ozone content and a wind-speed of $7.2\,m/s$). The latters can be improved by collecting meteorological data. Bias due to extreme geometrical conditions or to eventual adjacency effects could be tacked if a larger database was generated to conducting a statistical investigation on these parameters. Here, all the analyses were completed in the principal plane, but the CIMEL measurements in the almucantar geometry should allow to populate the database and to study specific parameters such as the vertical distribution of particles, the adjacency effects and the geometrical conditions. The spectral extrapolation of the IOP's from the red to the visible region needs to be validated. For that, a strategy would consist to predict the sky radiances at $440\,nm$ and to compare them with the CIMEL measurements.

The angular extrapolation of the optical properties to the near-backscattering region has to be also checked. This could be achieved by using MERIS data in the angular scattering domain $[150-180]\,deg.$, and in the near-infrared region (over black ocean). Simultaneous CIMEL data would indicate what will be the new aerosol model, and the radiances simulated at TOA with this model would be then compared with MERIS level-1*b* radiances. As far as we can rely on the MERIS radiometric calibration, this comparison would validate the IOP's at least in the red and near-infrared regions. It can be envisaged to use the MERIS backscattering measurements combined with the CIMEL sky radiances, to retrieve the aerosol phase function at the scattering angles which are not accessible from the ground. Other possibilities would be to use simultaneous CIMEL data sequences and measurements from multi-view sensors such as POLDER (POLarization and Directionality of Earth's Reflectances), MISR (Multi-angle Imaging Spectro-Radiometer) or AATSR (Advanced Along-Track Scanning Radiometer).

We conducted a first attempt to evaluate our approach through the comparison between simultaneous AOT's derived from MERIS and CIMEL. Although some preliminary results are encouraging, they need to be deeply investigated on a more extensive data set for the validation. The objective to propose a strategy for generating new LUT's is reached to be implemented for testing in the current MERIS algorithm. The latter will allow to fully validate our protocol.

Of course, the general approach used here over ocean will can be duplicated as well over land.

ACKNOWLEDGMENTS

This work has been financially supported by the European Space Agency (ESA). The authors would like to thank ACRI for providing the MERIS database.

REFERENCES

[1] Santer, R., V. Carrère, P. Dubuisson, and J.C. Roger. Atmospheric corrections over land for MERIS, *International Journal of Remote Sensing*, 20 (9), 1819-1840, 1999.

[2] Antoine, D., and A. Morel. A multiple scattering algorithm for atmospheric correction of remotely sensed ocean color (MERIS instrument): Principle and implementation for atmospheres carrying various aerosols including absorbing ones, *International Journal of Remote Sensing*, 20 (9), 1875-1916, 1999.

[3] Santer, R., and N. Martiny. Sky radiance measurements for ocean colour calibration-validation, *Applied Optics*, 42 (6), 896-907, 2003.

[4] Martiny, N., R Santer, and I. Smolskaia. Vicarious calibration of MERIS over dark waters in the near-infrared, *Journal of Remote Sensing and Environment*, 94 (4), 475-490, 2005.

[5] Santer, R., and F. Zagolski. Iterative process to derive aerosol phase function from CIMEL measurements, *submitted to International Journal of Remote Sensing by May* 2006.

[6] Deuzé, J.L., M. Herman, and R. Santer. Fourier series expansion of the transfer equation in the atmosphere-ocean system, *Journal of Quantitative Spectroscopy & Radiative Transfer*, 41 (6), 483-494, 1989.

[7] Holben, B., T. Eck, I. Slutsker, D. Tanré, J.P. Buis, A. Setzer, E. Vermote, J. Reagan, Y. Kaufman, T. Nakajima, F. Lavenu, I. Jankowiak, and A. Smirnov. AERONET – A federated instrument network and data archive for aerosol characterization, *Remote Sensing of Environment*, 66, 1-16, 1998.

[8] Chomko, R., and H.R. Gordon. Atmospheric correction of ocean color imagery: Use of the *Junge* power-law aerosol size distribution with variable refractive index to handle aerosol absorption, *Applied Optics*, *37*, 5560-5572, 1998.

[9] Zagolski, F., R. Santer, J. Vidot, and F. Thieuleux. Validation of the MERIS atmospheric correction over water using ground-based measurements of the solar extinction and of the sky radiances, *Proceedings of ENVISAT/MERIS-AATSR (ESA / ESRIN)*, Frascati, Italy, September 26-30, 2005.